Journal of Computational Applied Mechanics 2023, 54 (2): 167-185

DOI: 10.22059/JCAMECH.2022.351892.781

RESEARCH PAPER

Analytical Elasticity Solution for Accurate Prediction of Stresses in a Rectangular Plate Bending Analysis Using Exact 3-D Theory

Festus Chukwudi Onyeka [a], Thompson Edozie Okeke [b], Chidobere David Nwa-David [c], Benjamin Okwudili Mama [b,*]

[a] *Department of Civil Engineering, Edo State University Uzairue, Edo State, 312102, Nigeria.*
[b] *Department of Civil Engineering, University of Nigeria, Nsukka, Enugu State, 410101, Nigeria.*
[c] *Department of Civil Engineering, Michael Okpara University of Agriculture, Umudike, Abia State, 440109, Nigeria*

Abstract

The bending attributes of a uniformly-loaded thick plate was modelled with three-dimensional (3-D) elasticity plate theory using exact polynomial displacement functions. Plates with free-support at its third edge and simply-supported at other edges (SSFS), were covered in this study. The effect of shear-deformation along with the transverse normal strain-stress were considered in this model obviating the coefficients of shear correction. The total potential energy expression was formulated from 3-D kinematic and constitutive relations. The slope and deflection relationship were obtained from the equilibrium equation developed for the energy functional transformation. The solution of the equilibrium equation produced exact polynomial deflection function while the coefficient of deflection of the plate was formed from the governing equation employing a direct variation approach. The formula for computing the displacement-stress components of the plate was established from these solutions in order to evaluate the bending properties of the plate. The result of the study is presented at the span-depth ratio considered were 4, 5, 10, 15, 20, 50, 100 and CPT, while length-breadth ratio captured were 1.0 and 2.0. It was discovered that the deflection (∪) decreases as the span-depth ratio (a/t) increases and a constant value of 0.0081 and 0.0112 were sustained at a span - depth ratio of 50 till CPT for length-breadth ratio of 1.0 and 2.0 whereas the stresses perpendicular to the y and z axis ($\sigma_{y,\text{ and }}\sigma_z$) maintained a constant value of 0.2561 and 0.2537, 0.2249 and -0.0004 a span - depth ratio of 50 and CPT. Here, the performance of the plate structure is affected in terms of its serviceability. The value of the shear stresses in the x-y plane (τ_{xy}) increased negatively as the span-depth ratio rises while the shear stresses in the x-z plane (τ_{xz}) decreased positively span-depth ratio of 4 to 50 and increased negatively in span-depth ratio of 100 and CPT. The total average percentage variation of the center deflection values obtained by Onyeka and Okeke, (2020) and Gwarah (2019), is 3.28%. This showed that at the 97 % confidence level, the 3-D model is most suitable and safe for analyzing the bending characteristics of thick plates unlike the 2-D RPTs. The solutions

* *Corresponding Author:* ORCID: https://orcid.org/0000-0002-2668-9753, Email: boniface.mama@unn.edu.ng

realized herein certifies that the 3-D model model gave a more accurate and reliable solution compared refined plate theories compared to refined plate theories applied by previous authors in the available literature. It can be ascertained that the 3-D elasticity model produced an exact and consistent solution and are recommended for the analysis of various categories of the plate.

Keywords: Exact 3-D theory; Polynomial shape function; SSFS thick plate; stress prediction; Analytical elasticity solution

1. Introduction

Three-dimensional structural elements with orders dimensions along x, y, and z axes known as plates, are widely applied as the fundamental component of bridges, automobiles, aircrafts, ship hulls, retaining walls, building slabs and roofs [1-3]. Plates can be quadrilateral, square, circular or rectangular in shape and they can be homogeneous, non-homogeneous, orthotropic, anisotropic or isotropic based on their integral materials [4, 5]. Plates can have simply-supported, clamped, free edge conditions or a combination of any. Based on their thickness, plates can either be thin, moderately-thick or thick [6, 7]. Taking a/t as the span-to-depth [8] counts rectangular plates with $a/t \leq 20$ as thick plate, $20 \leq a/t \leq 50$ as moderately-thick plate and $50 \leq a/t \leq 100$ as thin plate.

In engineering, the demand for thick plates has accelerated greatly over the years because of its entrancing attributes such as its economic benefits, propensity to resist heavy loads and being customized to desired structural features [9]. The adequate perspicacity of the failure form and structural trait is vital for economical, safe design and to improve the properties of thick plates. Thick plates can be thoroughly and generally examined through bending, vibration or buckling [10, 11]. External forces or lateral loads imposed on the plate structure often result to bending and this phenomenon becomes more defined as the plate deforms perpendicularly to its surface. This deformation continues as the induced load exceeds the critical [12, 13]. And so, the plate fails. The need to circumvent structural instability emanating from deformations and obtaining an exact solution with adequate attention to the bending mannerism of thick plates, validates the essence of this study.

The plight of instability resulting from bending can be solved using several theories formulated and deployed by diverse scholars. The theories include; the classical plate theory (CPT), also referred to as a Kirchhoff plate theory, refined plate theories (RPT), and three-dimensional theory (3-D). The RPTs consists of the first-order shear deformation plate theory (FSDT), the trigonometric shear deformation theories (TSDT) [14], exponential shear deformation theories (ESDT) [15], polynomial shear deformation theories (PSDT) [16] and the higher-order shear deformation plate theories (HSDT) [17].

CPT is inadequate to investigate the bending of thick plates since it neglects the transverse shear effects. FSDT was introduced to address the deficiency of CPT but correction factor was applied [18, 19] for it to give the desired outcome. Conversely, HSDTs [17, 20] without it, complies with the zero shear-stress conditions at the top and underside of the plates. For a typical 3D plate, RPTs offers an approximate solution due to the negligence of normal stress and strain along the thickness axis of the plate. These RPTs which are 2D plate theory, are inconsistent and unreliable. To achieve an exact bending solution for a typical thick plate, the 3-D model is needed and this justifies the essence of this work.

The investigation for bending can be accomplished numerically, analytically or through the energy method or assemblage of any [8, 21, 22]. At different positions of the plate surface, the remedy to the bending problem satisfies the support demands of the plate in the governing equations for the analytical approach which comprises of Integral transform, Eigen expansion, Naiver and Levy series [23, 24]. Kantorovich methods, Finite difference, Galerkin, Collocation, Bubnov-Galerkin, truncated double Fourier series, boundary element and Ritz methods are different forms of numerical approach whose solutions are often inexact [25, 26]. Energy approach whose total energy is same with the total of strain and potential energy/external work on the continuum [27, 28]; can be either analytical or numerical.

In this study, energy method in an analytical form with 3-D theory is applied to obtain exact bending solutions for thick plates with SSFS boundary condition. Exact polynomial displacement function was employed to determine the displacements (in-plane and out-of-plane), moments, and all the stresses at different points of plates. The impact of the aspect ratios (span-depth and length-breadth ratios) were also considered. Outstandingly, this study evaluates the deflection, shear stresses at x-y axis, x-z axis, y-z axis, the normal stresses along x, y, z co-ordinates produced due to the applied load on the plate, and the in-plane displacement in the direction of x and y coordinates; a feat that was not accomplished in preceding studies. In thick plate analysis, the nature of displacement functions applied is of great concern to engineers as scholars that used assumed shape functions obtained

approximate bending solutions. This gap is also bridged in this study.

2. Literature Review

A Navier-type analytical solution was obtained by Mantari and Soares [29] using HSDT with virtual work principle and an assumption of variation in the mechanical features of the plates in the thickness axis, for simply supported plates under transverse bi-sinusoidal loads. Although their study showed a level of accuracy compared to other shear deformation theory, the strain and stress along the thickness direction of the plate was not taken into consideration. Plates with SSFS support status were also not captured, as well as polynomial shape functions.

New inverse TSDT was developed by Bhaskar *et al.* [30] to get a finite element solution for bi-directional bending assessment of thick isotropic plates, considering the effects of transverse shear deflection and rotating inertia. From a dynamic version of virtual work principle, the dominant equations and edge conditions of the theory was derived. Their model showed precise predictions of stresses and displacements when juxtaposed with other HSDTs, but was unable to consider an analytical and three-dimensional approaches. SSFS thick plates were not considered.

Tash and Neya [31] determined the displacements-stresses of thick plates that are transversely simply supported with thickness variations, applying displacement-potential-functions. The authors applied variable separation approach to handle the governing equations which were of quadratic and fourth order, satisfying the exact support conditions. Their solution proved satisfactory when examined with the finite-element method but a 3 D theory was not employed and SSFS thick plates were not taken into account.

Ghugal and Gajbhiye [32], Sayyad and Ghugal [33] analyzed the displacements-stresses of plates with RPTs. The effect of shear and strain deformation was captured neglecting the application of shear correction elements connected with FSDTs. The state of zero shear transverse stresses was satisfactory. The authors didn't consider the 3-D plate theory with polynomial functions. Plates with SSFS boundary condition were neglected.

Onyeka *et al.* [34] applied RPT of third order to obtain the in-plane displacements, deflections, shear force, bending moments and shear-deformation-rotations at arbitrary points on rectangular plates with CSCS edge conditions, using direct variational approach and polynomial displacement function. There was no consideration for SSFS thick plate and 3-D plate theory. Also, Onyeka *et al.* [1] applied polynomial displacement-shape function and RPTs to investigate the bending behavior of isotropic SSFS plates. The lateral critical imposed load was examined in their study. The authors did not use 3-D theory for their analysis.

RPT was utilized by Mantari *et al.* [14], Onyeka and Okeke [35] to obtain the displacement and stresses in thick rectangular plate. Polynomial function with 2D plate theory was applied in [35], while trigonometric theory was applied in [14]. The solutions obtained by these authors were inexact as the stresses along the thickness axis were not analyzed. Plates with the SSFS boundary condition were also neglected.

Onyeka and Okeke [36] considered SSFS plate and direct energy method in their bending analysis. The authors engaged both trigonometric and polynomial displacement functions to formulate the governing differential equation. The deflection and stresses obtained in their study were in good agreement with the other RPTs. The 3-D plate theory was not employed in their study.

Grigorenko *et al.* [37] applied Spline-collocation method with two-coordinate directions and a numerical approach based on the 3-D theory to get the bending solutions of a thick plate. The displacements-stresses in clamped plates were determined. The value for out-of-plane displacements at any given point in the plate cannot be accurately examined from by their approach. Plates with SSFS support-condition were not taken into consideration.

A 3-D trigonometric model was developed by Onyeka *et al.* [38], Onyeka and Mama [39] to solve the bending issue of isotropic thick CCCS and SSSS plates respectively. The equilibrium equations and total energy functional were formulated from 3-D kinematic and constitutive relations. The Excellency of 3-D theory in the thick plate analytic investigation was captured in their studies, but the authors did not address SSFS plates and polynomial shape functions were not applied in their analysis.

Hadi *et al.* [40] used the 3-D theory to analyze the bending features of functionally graded rectangular plates with variable exponential properties. The impact of different functionally-graded inequality on the stress and displacement fields was studied numerically. Significant effects of the properties graded-material on the plate's behavior was observed. The exact solutions of the stresses-displacements were also presented. The authors did not consider SSF-bounded rectangular plates and polynomial functions.

Non-classical elasticity models have been employed by most researchers to analyze plates. These scholars include: Rahmani *et al.* [41], Ebrahimi and Haghi [42], Nejad *et al.* [43], Yüksel and Akbaş [44-46]. Their studies were centered on functionally graded materials (FGM) and some considered non-classical elasticity theories. There was no consideration for isotropic rectangular SSFS plates, bending attributes and three-dimensional plate elasticity theory. Their attention was more on nanostructures using nonlocal elasticity, strain gradient and nonlocal strain gradient theory. Most of these past scholars neither analyze stresses for the bending attributes nor capture isotropic

rectangular plates in their work. The three-dimensional plate theory and SSFS boundary terms were not also considered.

Meanwhile, there few other past scholars that studied the analysis of isotropic plate material [47, 48] except Akbas [94] that worked on the bending analysis of a nano plate using generalized differential quadrature method while Akbas [95] did the study on the buckling of non-homogenous porous plate using the same approach. Both authors did not analyze the stresses along the thickness axis of the plate making their solution approximate.

The majority of the reported studies showed that many scholars analyzed bending of rectangular plates using refined plate theories without understanding that a plate is a three dimensional element with varying thickness while very few considered the application of 3-D plate theory. Those that considered a 3-D plate theory also could not capture the use of polynomial functions which, unlike trigonometry and exponential function is easier to apply to give solution of any type of edge condition such as SSFS plate. The exigency to address this research gap validates the usefulness of this study.

The solutions obtained by most researchers were limited to inexact due to the application of assumed displacement-shape functions. These functions were not derived from the governing equilibrium equation in a bid to avoid laborious mathematical analysis. The advantage of this study over the past work is its ability to handle all these shortcoming as it employs the exact displacement function to obtain its close-form solution for safe and cost-effective analysis.

Though several authors have carried out studies on the bending of rectangular plates, their solutions were mostly approximate and all the stress elements were not analyzed thereby making it difficult to estimate the exact function from the governing differential equation and at the same time satisfy exactly the specified conditions of the edges. Meanwhile, a complete 3-D plate theory as applied in this study is required to overcome the limitations of the previous studies. The displacements and stresses of SSFS thick plate are determined in this work using exact polynomial-displacement function and the 3-D model.

The physical interpretation of SSFS plate is that, the three edges of the plate are supported by a hinge and roller while the remaining one is free of support (hang without support. Eg. Cantilever) and continuous over the span of the plate. None of the edge is supported by a beam. This makes the study very significant because the such boundary condition (BC) exists depending on the type of hinged, roller or column support on the plate structure, thus, whenever such BC occurs it ought to be analyzed a such to ensure that it account for all the forces (stresses) acting on it. This is because, forces are generated due to the applied load on the structure, thereby will introduce significant errors in the result if they account for. Hence, the essence of the case study.

3. Research Methodology

3.1. Model Formulation

A The research methodology of this study is presented by considering a rectangular plate in the Figure 1 as a three-dimensional element in which the deformation exists in the three axis: length (a), width (b) and thickness (t). The analytical approach of energy method was used to obtain formulas for the analysis. The 3-D kinematics and constitutive relations for a static elastic theory of plate was used to formulate the governing equations which enables development of the formulae for the analysis.

3.2. Kinematics

The kinematics of the study if formulated by taking the assumption of the plate that the x-z section and y-z section, is no longer normal to x-y plane after bending.

Considering the elementary section of the plate in the figure 2, the Pythagoras theorem was was used to obtain the value of slope with respect to the in-plane displacement of the plate for small angle after bending of plate as follows:

$$\emptyset_x = \frac{\partial p}{\partial z} \tag{1}$$

$$\emptyset_y = \frac{\partial q}{\partial z} \tag{2}$$

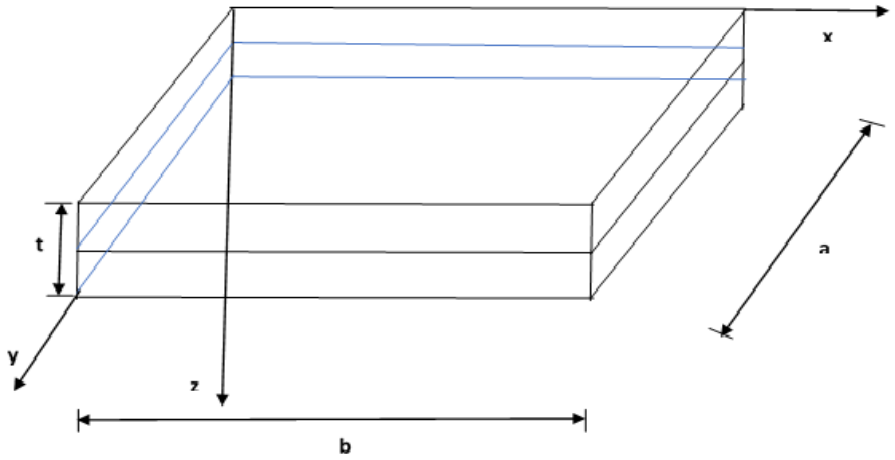

Fig. 1: An element of thick rectangular plate showing middle surface

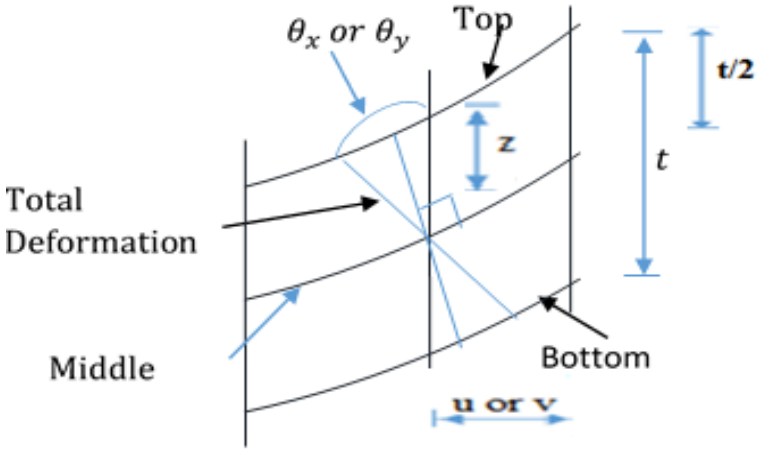

Fig. 2: Deformation of x-z (or y-z) section of plate after bending

Thus, the 3-D displacement kinematics along x, y and z axis are obtained in line with the work of Onyeka *et al.* [2], as:

$$p = z.\emptyset_x \tag{3}$$

$$q = z.\emptyset_y \tag{4}$$

Given that:

$$z = kt \tag{5}$$

$$\beta = \frac{a}{t} \tag{6}$$

$$\gamma = \frac{b}{a} \tag{7}$$

After substituting Equations (5), (6), and (7) the shear deformation slope become:

$$\emptyset_x = \frac{1}{t}.\frac{\partial p}{\partial k} \tag{8}$$

$$\emptyset_y = \frac{1}{t}.\frac{\partial q}{\partial k} \tag{9}$$

The strain and shear strain components are defined based on the theory of elasticity as the ratios of displacement of finite length of a plate to that of the finite length. They summarized as:

$$\varepsilon_x = \frac{\partial p}{\partial x} \tag{10}$$

$$\varepsilon_y = \frac{\partial q}{\partial y} \tag{11}$$

$$\varepsilon_z = \frac{\partial \cup}{\partial z} \tag{12}$$

$$\gamma_{xy} = \frac{\partial p}{\partial y} - \frac{\partial q}{\partial x} \tag{13}$$

$$\gamma_{xz} = \frac{\partial p}{\partial z} - \frac{\partial \cup}{\partial x} \tag{14}$$

$$\gamma_{yz} = \frac{\partial q}{\partial z} - \frac{\partial \cup}{\partial y} \tag{15}$$

After substituting Equations (5), (6) and (7), the six non-dimensional coordinates strain components were derived using strain-displacement expression according to Hooke's law and presented in Equation (13) - (18):

$$\varepsilon_x = \frac{\mathbf{1}}{\mathbf{a}} \cdot \frac{\boldsymbol{\partial p}}{\boldsymbol{\partial u}} \tag{16}$$

$$\varepsilon_y = \frac{\mathbf{1}}{\mathbf{a\gamma}} \cdot \frac{\boldsymbol{\partial q}}{\boldsymbol{\partial v}} \tag{17}$$

$$\varepsilon_z = \frac{\mathbf{1}}{\mathbf{t}} \cdot \frac{\boldsymbol{\partial \cup}}{\boldsymbol{\partial k}} \tag{18}$$

$$\gamma_{xy} = \frac{\mathbf{1}}{\mathbf{a}} \cdot \frac{\boldsymbol{\partial q}}{\boldsymbol{\partial u}} + \frac{\mathbf{1}}{\mathbf{a\gamma}} \cdot \frac{\boldsymbol{\partial p}}{\boldsymbol{\partial v}} \tag{19}$$

$$\gamma_{xz} = \frac{\mathbf{1}}{\mathbf{a}} \cdot \frac{\boldsymbol{\partial \cup}}{\boldsymbol{\partial u}} + \frac{\mathbf{1}}{\mathbf{t}} \cdot \frac{\boldsymbol{\partial p}}{\boldsymbol{\partial k}} \tag{20}$$

$$\gamma_{yz} = \frac{\mathbf{1}}{\mathbf{a\gamma}} \cdot \frac{\boldsymbol{\partial \cup}}{\boldsymbol{\partial v}} + \frac{\mathbf{1}}{\mathbf{t}} \cdot \frac{\boldsymbol{\partial q}}{\boldsymbol{\partial k}} \tag{21}$$

3.3. Constitutive Relations

The three dimensional constitutive relation for isotropic material is given as:

$$\begin{bmatrix} \boldsymbol{\varepsilon_x} \\ \boldsymbol{\varepsilon_y} \\ \boldsymbol{\varepsilon_z} \\ \boldsymbol{\gamma_{xz}} \\ \boldsymbol{\gamma_{yz}} \\ \boldsymbol{\gamma_{xy}} \end{bmatrix} = \frac{1}{E} \begin{bmatrix} \mathbf{1} & -\boldsymbol{\mu} & -\boldsymbol{\mu} & \mathbf{0} & \mathbf{0} & \mathbf{0} \\ -\boldsymbol{\mu} & \mathbf{1} & -\boldsymbol{\mu} & \mathbf{0} & \mathbf{0} & \mathbf{0} \\ -\boldsymbol{\mu} & -\boldsymbol{\mu} & \mathbf{1} & \mathbf{0} & \mathbf{0} & \mathbf{0} \\ \mathbf{0} & \mathbf{0} & \mathbf{0} & \mathbf{2(1+\mu)} & \mathbf{0} & \mathbf{0} \\ \mathbf{0} & \mathbf{0} & \mathbf{0} & \mathbf{0} & \mathbf{2(1+\mu)} & \mathbf{0} \\ \mathbf{0} & \mathbf{0} & \mathbf{0} & \mathbf{0} & \mathbf{0} & \mathbf{2(1+\mu)} \end{bmatrix} \begin{bmatrix} \boldsymbol{\sigma_x} \\ \boldsymbol{\sigma_y} \\ \boldsymbol{\sigma_z} \\ \boldsymbol{\tau_{xz}} \\ \boldsymbol{\tau_{yz}} \\ \boldsymbol{\tau_{xy}} \end{bmatrix} \tag{22}$$

The six stress components were obtained by substituting Equations 16 to 21 into Equation 22 and simplifying the

outcome gave:

$$\sigma_x = \left[\mu\frac{\mathbf{kt}}{\boldsymbol{\gamma a}} * \frac{\partial \emptyset_y}{\partial v} + (\mathbf{1}-\boldsymbol{\mu})\,\frac{\mathbf{kt}}{\mathbf{a}} * \frac{\partial \emptyset_x}{\partial u} + \mu\frac{\mathbf{1}}{\mathbf{t}} * \frac{\partial \cup}{\partial \mathbf{k}}\right]\frac{\mathbf{E}}{(\mathbf{1}+\boldsymbol{\mu})(\mathbf{1}-\mathbf{2}\boldsymbol{\mu})} \quad (23)$$

$$\sigma_y = \left[\mu\mathbf{kt} * \frac{\partial \emptyset_x}{\boldsymbol{a}\partial \boldsymbol{u}} + \frac{\mu}{\boldsymbol{t}} * \frac{\partial \cup}{\partial \boldsymbol{k}} + \frac{(\mathbf{1}-\boldsymbol{\mu})\mathbf{kt}}{\boldsymbol{\gamma a}} * \frac{\partial \emptyset_y}{\partial \boldsymbol{v}}\right]\frac{\mathbf{E}}{(\mathbf{1}+\boldsymbol{\mu})(\mathbf{1}-\mathbf{2}\boldsymbol{\mu})} \quad (24)$$

$$\sigma_z = \left[\frac{\mu\mathbf{kt}}{\boldsymbol{\gamma a}} * \frac{\partial \emptyset_y}{\partial \boldsymbol{v}} + \frac{(\mathbf{1}-\boldsymbol{\mu})}{\boldsymbol{t}} * \frac{\partial \cup}{\partial \boldsymbol{k}} + \mu\mathbf{kt} * \frac{\partial \emptyset_x}{\boldsymbol{a}\partial \boldsymbol{u}}\right]\frac{\mathbf{E}}{(\mathbf{1}+\boldsymbol{\mu})(\mathbf{1}-\mathbf{2}\boldsymbol{\mu})} \quad (25)$$

$$\tau_{xy} = \left[\frac{\mathbf{kt}\partial \emptyset_y}{\boldsymbol{a2}\partial \boldsymbol{u}} * \frac{\mathbf{kt}}{\mathbf{2}\boldsymbol{\gamma a}}\frac{\partial \emptyset_x}{\partial \boldsymbol{v}}\right]\frac{\boldsymbol{E}(\mathbf{1}-\mathbf{2}\mu)}{(\mathbf{1}+\boldsymbol{\mu})(\mathbf{1}-\mathbf{2}\boldsymbol{\mu})} \quad (26)$$

$$\tau_{yz} = \left[\frac{\mathbf{1}}{\boldsymbol{a2\gamma}}\frac{\partial \cup}{\partial \boldsymbol{Q}} + \frac{\emptyset_y}{\mathbf{2}}\right]\frac{(\mathbf{1}-\mathbf{2}\mu)\boldsymbol{E}}{(\mathbf{1}+\boldsymbol{\mu})(\mathbf{1}-\mathbf{2}\boldsymbol{\mu})} \quad (27)$$

$$\tau_{xz} = \left[\frac{\mathbf{1}}{\boldsymbol{a}}\frac{\partial \cup}{\mathbf{2}\partial \boldsymbol{u}} + \frac{\emptyset_x}{\mathbf{2}}\right]\frac{(\mathbf{1}-\mathbf{2}\mu)\boldsymbol{E}}{(\mathbf{1}+\boldsymbol{\mu})(\mathbf{1}-\mathbf{2}\boldsymbol{\mu})} \quad (28)$$

3.4. Formulation of Energy

The potential energy which is summation of all the external work done on the body of the material and strain energy generated due to the applied load on the plate is mathematically defined as:

$$\nexists = \in - \ni \quad (29)$$

Given that;

$$\ni = \boldsymbol{wab} \cap \int_0^1 \int_0^1 \complement\, \boldsymbol{du}\, \boldsymbol{dv} \quad (30)$$

And;

$$\in = \frac{\boldsymbol{tab}}{\mathbf{2}} \int_0^1 \int_0^1 \int_{-0.5}^{0.5} \left(\sigma_x \varepsilon_x + \sigma_y \varepsilon_y + \sigma_z \varepsilon_z + \boldsymbol{\tau}_{xy}\gamma_{xy} + \boldsymbol{\tau}_{xz}\gamma_{xz} + \boldsymbol{\tau}_{yz}\gamma_{yz}\right) \boldsymbol{du}\, \boldsymbol{dv}\, \boldsymbol{dk} \quad (31)$$

Substituting Equations 30 and 31 into Equation 29 to get the energy equation as:

$$\begin{aligned}\nexists = \frac{\mathbf{Et}^3\boldsymbol{\gamma}}{\mathbf{24}(\mathbf{1}+\boldsymbol{\mu})(\mathbf{1}-\mathbf{2}\boldsymbol{\mu})} \int_0^1 \int_0^1 \Bigg[& \left(\frac{\partial \emptyset_y}{\partial \boldsymbol{u}}\right)^2 \frac{(\mathbf{1}-\mathbf{2}\mu)}{\mathbf{2}} + \frac{\mathbf{1}}{\boldsymbol{\gamma}}\frac{\partial \emptyset_x}{\partial \boldsymbol{u}} * \frac{\partial \emptyset_y}{\partial \boldsymbol{v}} + \frac{(\mathbf{1}-\boldsymbol{\mu})}{\boldsymbol{\gamma}^2}\left(\frac{\partial \emptyset_y}{\partial \boldsymbol{v}}\right)^2 + \frac{(\mathbf{1}-\boldsymbol{\mu})}{\boldsymbol{t}^2} \\ & * \left(\frac{\partial \cup}{\partial \boldsymbol{k}}\right)^2 \boldsymbol{\beta}^2 + \frac{(\mathbf{1}-\mathbf{2}\mu)}{\mathbf{2}\boldsymbol{\gamma}^2}\left(\frac{\partial \emptyset_x}{\partial \boldsymbol{v}}\right)^2 \\ & + \frac{\mathbf{6}(\mathbf{1}-\mathbf{2}\mu)}{\boldsymbol{t}^2}\Bigg\{\boldsymbol{a}^2 {\emptyset_x}^2 + \left(\frac{\partial \cup}{\partial \boldsymbol{u}}\right)^2 + \boldsymbol{a}^2 {\emptyset_y}^2 + \left(\frac{\partial \cup}{\partial \boldsymbol{v}}\right)^2 \frac{\mathbf{1}}{\boldsymbol{\gamma}^2} + \boldsymbol{a}\left(\frac{\partial \cup}{\partial \boldsymbol{u}}\right) \mathbf{2}\emptyset_x \\ & + \left(\frac{\partial \cup}{\partial \boldsymbol{v}}\right) \boldsymbol{2a} * \frac{\emptyset_y}{\boldsymbol{\gamma}}\Bigg\} + \left(\frac{\partial \emptyset_x}{\partial \boldsymbol{u}}\right)^2 (\mathbf{1}-\boldsymbol{\mu})\Bigg] \boldsymbol{\partial u \partial v} - \boldsymbol{w\gamma a}^2 \int_0^1 \int_0^1 \complement \boldsymbol{S}\, \boldsymbol{\partial u \partial v}\end{aligned} \quad (32)$$

3.5. Solution to the Equilibrium Equation

The two compatibility equations were obtained by minimizing the total potential energy functional with respect to rotations in x-z and in y-z plane to give:

$$\frac{\mathbf{Et^3\gamma}}{\mathbf{24(1+\mu)(1-2\mu)}}\int_0^1\int_0^1\left[\mathbf{2(1-\mu)}\frac{\boldsymbol{\partial^2\emptyset_x}}{\boldsymbol{\partial u^2}}+\frac{\boldsymbol{\partial^2\emptyset_y}}{\boldsymbol{\partial u\partial v}}*\frac{\mathbf{1}}{\boldsymbol{\gamma}}+\frac{\mathbf{(1-2\mu)}}{\boldsymbol{\gamma^2}}\frac{\boldsymbol{\partial^2\emptyset_x}}{\boldsymbol{\partial v^2}}+\left(\mathbf{2a^2\theta_{sx}}+\mathbf{2a.}\frac{\boldsymbol{\partial}\cup}{\boldsymbol{\partial u}}\right)\frac{\mathbf{6(1-2\mu)}}{\mathbf{t^2}}\right]\boldsymbol{\partial u\partial v}=\mathbf{0} \tag{33}$$

$$\frac{\mathbf{Et^3\gamma}}{\mathbf{24(1+\mu)(1-2\mu)}}\int_0^1\int_0^1\left[\frac{\boldsymbol{\partial^2\emptyset_x}}{\boldsymbol{\partial u\partial v}}*\frac{\mathbf{1}}{\boldsymbol{\gamma}}+\mathbf{2}\frac{\boldsymbol{\partial^2\emptyset_y}}{\boldsymbol{\partial v^2}}*\frac{\mathbf{(1-\mu)}}{\boldsymbol{\gamma^2}}+\mathbf{2}\frac{\mathbf{(1-2\mu)}}{\mathbf{2}}\frac{\boldsymbol{\partial^2\emptyset_y}}{\boldsymbol{\partial u^2}}+\left(\mathbf{2a^2\emptyset_y}+\frac{\mathbf{2a.}\boldsymbol{\partial}\cup}{\boldsymbol{\gamma}\ \boldsymbol{\partial v}}\right)\frac{\mathbf{6(1-2\mu)}}{\mathbf{t^2}}\right]\boldsymbol{\partial u\partial v}=\mathbf{0} \tag{34}$$

The solution of the equilibrium differential equation gives the characteristics polynomial displacement and rotation functions as presented in the Equation 35-37 as:

$$\cup = H_0[(1\ \ u\ \ u^2\ \ u^3\ \ u^4)\begin{bmatrix}\alpha_0\\ \alpha_1\\ \alpha_2\\ \alpha_3\\ \alpha_4\end{bmatrix}.(1\ \ v\ \ v^2\ \ v^3\ \ v^4)\begin{bmatrix}b_0\\ b_1\\ b_2\\ b_3\\ b_4\end{bmatrix}] \tag{35}$$

$$\emptyset_x = \frac{c}{\alpha}.H_0[(1\ \ 2R\ \ 3R^2\ \ 4R^3)\begin{bmatrix}\alpha_1\\ \alpha_2\\ \alpha_3\\ \alpha_4\end{bmatrix}.(1\ \ Q\ \ Q^2\ \ Q^3\ \ Q^4)\begin{bmatrix}b_0\\ b_1\\ b_2\\ b_3\\ b_4\end{bmatrix}] \tag{36}$$

$$\emptyset_y = \frac{c}{\alpha\beta}.H_0[(1\ \ R\ \ R^2\ \ R^3\ \ R^4)\begin{bmatrix}\alpha_0\\ \alpha_1\\ \alpha_2\\ \alpha_3\\ \alpha_4\end{bmatrix}.(1\ \ 2Q\ \ 3Q^2\ \ 4Q^3)\begin{bmatrix}b_1\\ b_2\\ b_3\\ b_4\end{bmatrix}] \tag{37}$$

Considering a transversely loaded rectangular thick plate whose Poisson's ratio is 0.3 under uniformly distributed load as shown in the Figure 2, the derived trigonometric deflection functions is subjected to a SSFS boundary condition to get the particular solution of the deflection functions is subjected to a SSFS boundary condition to get the particular solution of the deflection

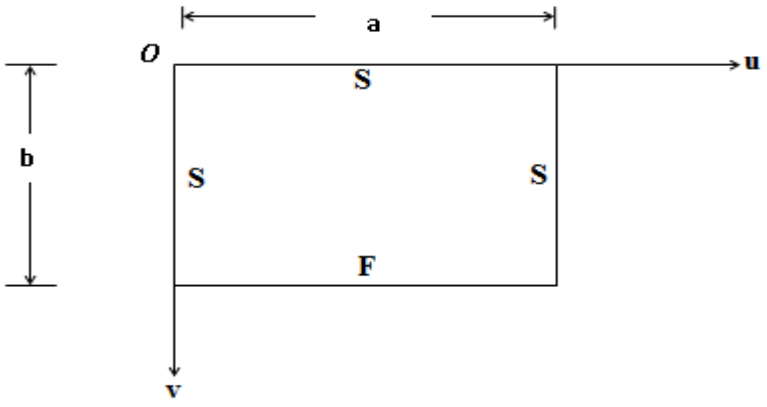

Fig. 3: SSFS Rectangular Plate

Applying the initial conditions of the plate in Figure 2, the relationship between the displacement and shape function of the plate as:

$$\cup = \mathrm{C}.\cap \tag{38}$$

$$\emptyset_x = \frac{\boldsymbol{h}}{\boldsymbol{a}}.\frac{\partial \mathrm{C}}{\partial \boldsymbol{u}} \tag{39}$$

$$\emptyset_y = \frac{\boldsymbol{g}}{\boldsymbol{\gamma a}}.\frac{\partial \mathrm{C}}{\partial \boldsymbol{v}} \tag{40}$$

The in polynomial form of the shape function of the plate after satisfying the boundary conditions is given as:

$$\mathrm{C} = \left(u - 2u^3 + u^4\right) \times \left(\frac{7v}{3} - \frac{10}{3}v^3 + \frac{10}{3}v^4 - v^5\right) \tag{41}$$

Substituting Equation 38, 39, 40, 30 and 31 into 29, gives:

$$\begin{aligned} \nexists = \frac{\mathbf{E}\boldsymbol{t}^3\boldsymbol{\gamma}}{\mathbf{24}(\mathbf{1}+\mu)(\mathbf{1}-\mathbf{2}\mu)}\Bigg[&(\mathbf{1}-\mu)\boldsymbol{h}^2\boldsymbol{r}_x + \frac{\mathbf{1}}{\boldsymbol{\gamma}^2}\left[\boldsymbol{h}.\boldsymbol{g} + \frac{(\mathbf{1}-\mathbf{2}\mu)\boldsymbol{h}^2}{\mathbf{2}} + \frac{(\mathbf{1}-\mathbf{2}\mu)\boldsymbol{g}^2}{\mathbf{2}}\right]\boldsymbol{r}_{xy} \\ &+ \frac{(\mathbf{1}-\mu)\boldsymbol{g}^2}{\boldsymbol{\gamma}^4}\boldsymbol{r}_y \\ &+ \mathbf{6}(\mathbf{1}-\mathbf{2}\mu)\boldsymbol{\beta}^2\left([\boldsymbol{h}^2 + \cap^2 + \mathbf{2}\cap\boldsymbol{h}].\boldsymbol{r}_z + \frac{\mathbf{1}}{\boldsymbol{\gamma}^2}.[\boldsymbol{g}^2 + \cap^2 + \mathbf{2}\cap\boldsymbol{g}].\boldsymbol{r}_{2z}\right) \\ &- \frac{\mathbf{2}\boldsymbol{q}\boldsymbol{a}^4\boldsymbol{r}_c\cap}{\boldsymbol{D}^*}\Bigg] \end{aligned} \tag{42}$$

Where:

$$\boldsymbol{r}_x = \int_0^1\int_0^1 \left(\frac{\partial^2 \mathrm{C}}{\partial \boldsymbol{u}^2}\right)^2 \partial \boldsymbol{u}\partial \boldsymbol{v} \tag{43}$$

$$\boldsymbol{r}_{xy} = \int_0^1\int_0^1 \left(\frac{\partial^2 \mathrm{C}}{\partial \boldsymbol{u}\partial \boldsymbol{v}}\right)^2 \partial \boldsymbol{u}\partial \boldsymbol{v} \tag{44}$$

$$r_y = \int_0^1 \int_0^1 \left(\frac{\partial^2 C}{\partial v^2}\right)^2 \partial u \partial v \tag{45}$$

$$r_z = \int_0^1 \int_0^1 \left(\frac{\partial C}{\partial u}\right)^2 \partial u \partial v \tag{46}$$

$$r_{2z} = \int_0^1 \int_0^1 \left(\frac{\partial C}{\partial v}\right)^2 \partial u \partial v \tag{47}$$

$$r_c = \int_0^1 \int_0^1 C \, \partial u \partial v \tag{48}$$

Minimizing Equation 42 with respect to h gives:

$$\frac{1}{2\gamma^2}[g + h(1-2\mu)]r_{xy} + hr_x(1-\mu) = -6(1-2\mu)\beta^2[h + \cap].r_z \tag{49}$$

Minimizing Equation 42 with respect to g gives:

$$\frac{1}{2\gamma^2}[h + g(1-2\mu)]r_{xy} + \frac{(1-\mu)g}{\gamma^4}k_y = +\frac{6}{\gamma^2}(1-2\mu)\beta^2([g + \cap].r_{2z}) \tag{50}$$

Re-write the Equations (49) and (50) and simplifying to get Equations (51) and (52) as:

$$h = \cap \frac{(k_{12}k_{23} - k_{13}k_{22})}{(k_{12}k_{12} - k_{11}k_{22})} \tag{51}$$

$$g = \cap \frac{(k_{12}k_{13} - k_{11}k_{23})}{(k_{12}k_{12} - k_{11}k_{22})} \tag{52}$$

Where;

$$k_{11} = (1-\mu)r_x + \frac{1}{2\gamma^2}(1-2\mu)r_{xy} + 6(1-2\mu)\beta^2 r_z \tag{53}$$

$$k_{12} = k_{21} = \frac{1}{2\gamma^2}r_{xy};\ k_{13} = -6(1-2\mu)\beta^2 r_z \tag{54}$$

$$k_{22} = \frac{(1-\mu)}{\gamma^4}r_y + \frac{1}{2\gamma^2}(1-2\mu)r_{xy} + \frac{6}{\gamma^2}(1-2\mu)\beta^2 r_{2z} \tag{55}$$

$$k_{23} = k_{32} = -\frac{6}{\gamma^2}(1-2\mu)\beta^2 r_{2z} \tag{56}$$

Minimizing Equation 42 with respect to $\cap$ gives:

$$\frac{\mathbf{Et^3\gamma}}{\mathbf{24(1+\mu)(1-2\mu)}}\left[\mathbf{6(1-2\mu)\beta^2}\left(\mathbf{[2\cap+2h].r_z+\frac{1}{\gamma^2}.[2\cap+2g].r_{2z}}\right)\right] - \frac{\mathbf{24wa^4r_c(1+\mu)(1-2\mu)}}{\mathbf{Et^3}} = \mathbf{0} \tag{57}$$

$$\frac{\mathbf{(1-2\mu)\beta^2Et^3\gamma}}{\mathbf{4(1+\mu)(1-2\mu)}}\left\{\left[\cap+\cap\frac{\mathbf{(k_{12}k_{23}-k_{13}k_{22})}}{\mathbf{(k_{12}k_{12}-k_{11}k_{22})}}\right].r_z+\frac{1}{\beta^2}.\left[\cap+\cap\frac{\mathbf{(k_{12}k_{13}-k_{11}k_{23})}}{\mathbf{(k_{12}k_{12}-k_{11}k_{22})}}\right].r_{2z}\right\} = \frac{\mathbf{wa^4r_c(1+\mu)(1-2\mu)\beta^3}}{\mathbf{E}} \tag{58}$$

Factorizing Equations (58) and simplifying gives:

$$\cap = \frac{2q(1+\mu)(1-2\mu)\beta^3}{E}\left\{\frac{ar_c}{(1-2\mu)\left(\frac{a}{t}\right)^2\left(\left[1+\frac{(k_{12}k_{23}-k_{13}k_{22})}{(k_{12}k_{12}-k_{11}k_{22})}\right].r_z+\frac{1}{\beta^2}.\left[1+\frac{(k_{12}k_{13}-k_{11}k_{23})}{(k_{12}k_{12}-k_{11}k_{22})}\right].r_{2z}\right)}\right\} \tag{59}$$

3.6. Exact Displacement and Stress Expression

By substituting the value of $\cap$ in Equation 59 into Equation 41, the deflection equation after satisfying the boundary condition of SSFS plate is given as:

$$\cup = \cap\left(u-2u^3+u^4\right)\times\left(\frac{7v}{3}-\frac{10}{3}v^3+\frac{10}{3}v^4-v^5\right) \tag{60}$$

Similarly, the in-plane displacement along x-axis becomes:

$$p = \frac{(k_{12}k_{23}-k_{13}k_{22})}{(k_{12}k_{12}-k_{11}k_{22})}\left\{\frac{12q(1+\mu)(1-2\mu)\beta^2kr_c}{(1-2\mu)\left(\frac{a}{t}\right)^2\left(\left[1+\frac{(k_{12}k_{23}-k_{13}k_{22})}{(k_{12}k_{12}-k_{11}k_{22})}\right].r_z+\frac{1}{\beta^2}.\left[1+\frac{(k_{12}k_{13}-k_{11}k_{23})}{(k_{12}k_{12}-k_{11}k_{22})}\right].r_{2z}\right)}\right\}\frac{1}{E}\frac{\partial C}{\partial u} \tag{61}$$

$$\boldsymbol{p = \frac{12q(1+\mu)(1-2\mu)\beta^2}{E}\left(\frac{kMr_c}{L}\right)\frac{\partial C}{\partial u}} \tag{62}$$

Where;

$$\boldsymbol{L = 6(1-2\mu)\beta^2\left([1+h].r_z+\frac{1}{\gamma^2}.[1+g].r_{2z}\right)} \tag{63}$$

$$\boldsymbol{N = \frac{(r_{12}r_{23}-r_{13}r_{22})}{(r_{12}r_{12}-r_{11}r_{22})}} \tag{64}$$

$$\boldsymbol{M = \frac{(r_{12}r_{13}-r_{11}r_{23})}{(r_{12}r_{12}-r_{11}r_{22})}} \tag{65}$$

Similarly, the in-plane displacement along y-axis becomes;

$$\boldsymbol{q = \frac{12q(1+\mu)(1-2\mu)\beta}{E}\left(\frac{kNr_c}{L}\right)\frac{\partial C}{\partial v}} \tag{66}$$

The six stress elements after satisfying the boundary condition are presented in Equations (67)-(72) as:

$$\sigma_x = \frac{\mathbf{E}}{(1+\mu)(1-2\mu)}\left[\frac{\mathbf{k}}{\beta}.\frac{\partial^2 C}{\partial u^2}(1-\mu) + \mu\beta^4 * \frac{12q(1+\mu)(1-2\mu)}{E}\left(\frac{r_c}{L}\right)\frac{\partial C}{\partial k} + \frac{\mu k}{\gamma\beta}.\frac{\partial^2 C}{\partial v^2}\right] \quad (67)$$

$$\sigma_y = \frac{\mathbf{E}}{(1+\mu)(1-2\mu)}\left[\frac{\mu k}{\beta}.\frac{\partial^2 C}{\partial u^2} + \mu\beta^4 * \frac{12q(1+\mu)(1-2\mu)}{E}\left(\frac{r_c}{L}\right)\frac{\partial C}{\partial k} + \frac{(1-\mu)k}{\gamma\beta}.\frac{\partial^2 C}{\partial v^2}\right] \quad (68)$$

$$\sigma_z = \frac{\mathbf{E}}{(1+\mu)(1-2\mu)}\left[\frac{\mu k}{\beta}.\frac{\partial^2 C}{\partial u^2} + (1-\mu)\beta^4 * \frac{12q(1+\mu)(1-2\mu)}{\beta}\left(\frac{r_c}{L}\right)\frac{\partial C}{\partial k} + \frac{\mu k}{\gamma\beta}.\frac{\partial^2 C}{\partial v^2}\right] \quad (69)$$

$$\tau_{xy} = \frac{E(1-2\mu)}{(1+\mu)(1-2\mu)}.\left[\frac{\mathbf{k}}{2\beta}.\frac{\partial^2 \partial C}{\partial u \partial v} + \frac{\beta^2 \mathbf{k}}{2\alpha\gamma}.\frac{12q(1+\mu)(1-2\mu)}{E}\left(\frac{r_c}{L}\right)\frac{\partial^2 \partial C}{\partial u \partial v}\right] \quad (70)$$

$$\tau_{xz} = \frac{(1-2\mu)E}{(1+\mu)(1-2\mu)}.\left[\frac{1}{2}\frac{\partial C}{\partial u} + \frac{\beta^3}{2} * \frac{12q(1+\mu)(1-2\mu)}{E}\left(\frac{r_c}{L}\right)\frac{\partial C}{\partial u}\right] \quad (71)$$

$$\tau_{yz} = \frac{(1-2\mu)E}{(1+\mu)(1-2\mu)}\left[\frac{1}{2}\frac{\partial C}{\partial v} + \frac{\beta^3}{2\gamma} * \frac{12q(1+\mu)(1-2\mu)}{E}\left(\frac{r_c}{L}\right)\frac{\partial C}{\partial v}\right] \quad (72)$$

4. Results and Discussion

The numerical outcome for the non-dimensional values of displacements and stresses of SSFS thick plate, were obtained using exact polynomial displacement functions and direct variation approach with 3-D plate theory. Tables 1 to 2 and Figures 4 to 9 represents the variation of displacements, normal and shear stresses with different span-depth ratio of varying length-breadth ratio. The span-depth ratio considered were 4, 5, 10, 15, 20, 50, 100 and CPT, while length-breadth ratio captured were 1.0 and 2.0.

Table 1: Displacement and Stresses of SSFS plate (length/width = 1)

$\alpha = \frac{a}{t}$	U	p	Q	$\overline{\sigma_x}$	$\overline{\sigma_y}$	$\overline{\sigma_z}$	$\overline{\tau_{xy}}$	$\overline{\tau_{xz}}$	$\overline{\tau_{yz}}$
4	0.0099	-0.0136	-0.0057	0.5273	0.2821	0.2797	-0.1150	0.0193	0.0072
5	0.0093	-0.0132	-0.0054	0.5124	0.2726	0.2703	-0.1112	0.0122	0.0045
10	0.0084	-0.0126	-0.0051	0.1487	0.2602	0.2578	-0.1062	0.0029	0.0010
15	0.0082	-0.0125	-0.0051	0.4899	0.2579	0.2555	-0.1053	0.0012	0.0004
20	0.0082	-0.0125	-0.0051	0.4857	0.2571	0.2547	-0.1050	0.0006	0.0002
50	0.0081	-0.0124	-0.0051	0.4827	0.2563	0.2539	-0.1046	2.2E-06	-7E-05
100	0.0081	-0.0124	-0.0051	0.4825	0.2561	0.2537	-0.1046	-8.9E-05	-0.0001
CPT	0.0081	-0.0124	-0.0051	0.4824	0.2561	0.2537	-0.1046	-0.0001	-0.0001

Table 2: Displacement and Stresses of SSFS plate (length/width = 2)

$\alpha = \frac{a}{t}$	U	p	Q	$\overline{\sigma_x}$	$\overline{\sigma_y}$	$\overline{\sigma_z}$	$\overline{\tau_{xy}}$	$\overline{\tau_{xz}}$	$\overline{\tau_{yz}}$
4	0.0134	-0.0185	-0.0038	0.6751	0.2441	0.0041	-0.1003	0.0225	0.0043
5	0.0126	-0.0180	-0.0037	0.6559	0.2371	0.0025	-0.0974	0.0143	0.0027
10	0.0115	-0.0173	-3.6E-03	0.6307	0.2279	0.0003	-0.0937	0.0035	0.0006
15	0.0113	-0.0172	-3.5E-03	0.6261	0.2263	-5E-05	-0.093	0.0015	0.0002
20	0.0113	-1.7E-02	-3.5E-03	0.6245	0.2257	-0.0002	-0.0928	0.0008	5.5E-05
50	0.0112	-1.7E-02	-3.5E-03	0.6227	0.2250	-0.0003	-0.0925	2E-05	-9.2E-05
100	0.0112	-1.7E-02	-3.5E-03	0.6225	0.2249	-0.0004	-0.0925	-8E-05	-1.2E-04
CPT	0.0112	-1.7E-02	-3.5E-03	0.6224	0.2249	-0.0004	-0.0925	-0.0001	-1.1E-04

Table 1 and 2, Figures 4 and 5 reveals that the out-of-plane displacement (U) decreases as the span-depth ratio (a/t) increases and a constant value of 0.0081 and 0.0112 were sustained at a span - depth ratio of 50 till CPT for length-breadth ratio of 1.0 and 2.0 respectively. As the span-thickness ratio got higher, the in-plane displacement along x and y axis (p and q) increased in the negative direction. The difference in deflection (U) is high when the

plate is thicker and becomes little as it gets thinner when it is subjected to the same loading phenomenon. The reductions advance until the plate structure deflects away from the elastic yield stress engendering structural failure.

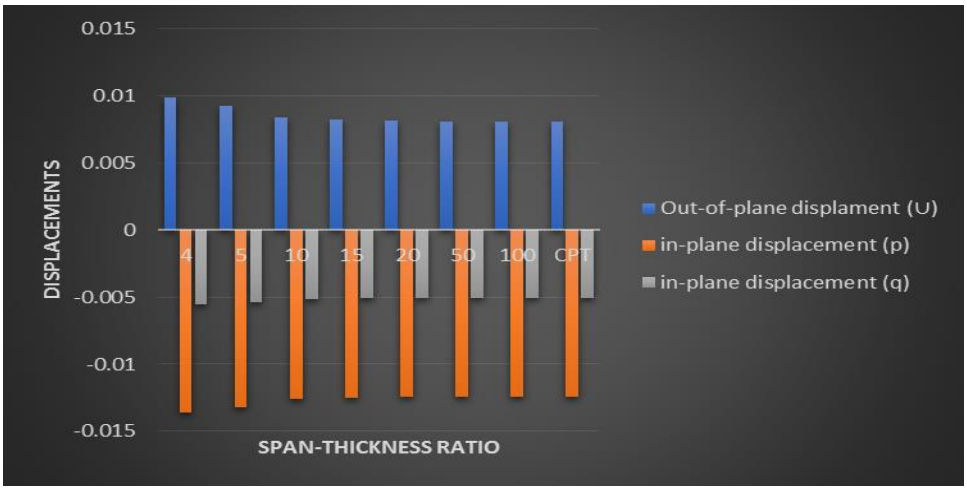

Fig. 4: Displacements and span-thickness ratio variation for SSFS plate with aspect ratio of 1.0

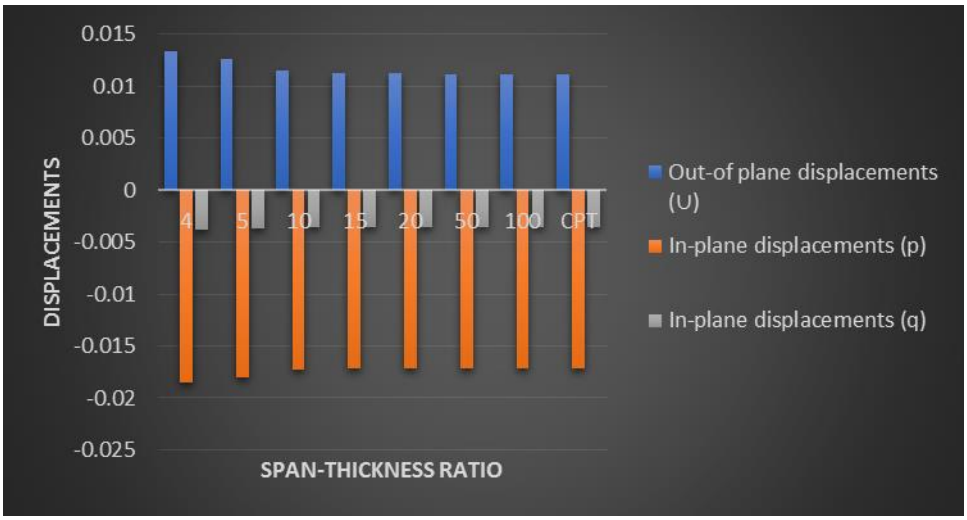

Fig. 5: Displacements and span-thickness ratio variation for SSFS plate with aspect ratio of 2.0

The non-dimensional parameters of normal stresses (σ_x, $\sigma_{y,\text{ and }}\sigma_z$) as presented in Table and 2, Figures 6 and 7 decreases as the span-depth ratio increases for each of the length-breadth ratio. The stresses perpendicular to the y and z axis ($\sigma_{y,\text{ and }}\sigma_z$) maintained a constant value of 0.2561 and 0.2537, 0.2249 and -0.0004 a span - depth ratio of 50 and CPT at length-breadth ratio of 1.0 and 2.0 respectively. Failure of the plate is bound to occur as more stresses are induced within the plate element, with the plate material being stretched beyond the elastic limit. The performance of the plate structure is affected in terms of its serviceability. Adequate consideration should be given during the selection of the thickness and other dimensions in the x and y axis of the plate to establish accuracy of the investigation and safety in construction.

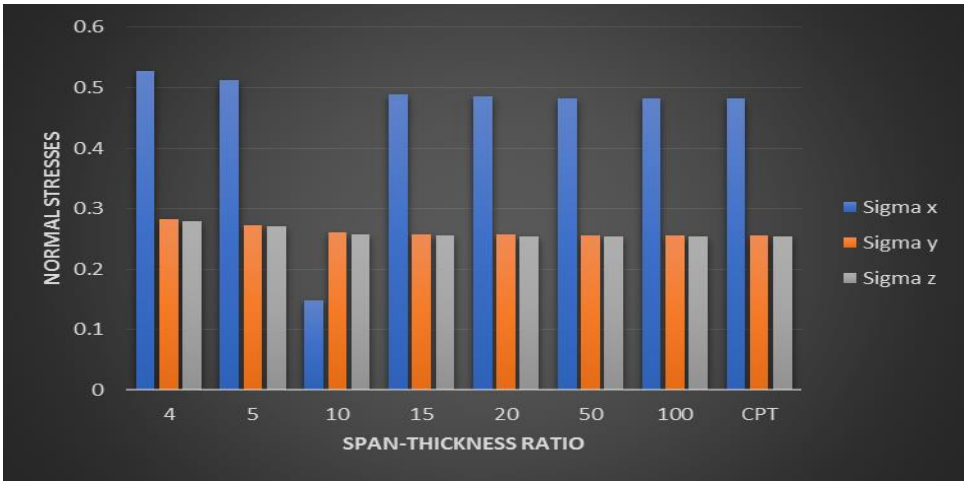

Fig. 6: Normal stresses and span-thickness ratio variation for SSFS plate with aspect ratio of 1.0

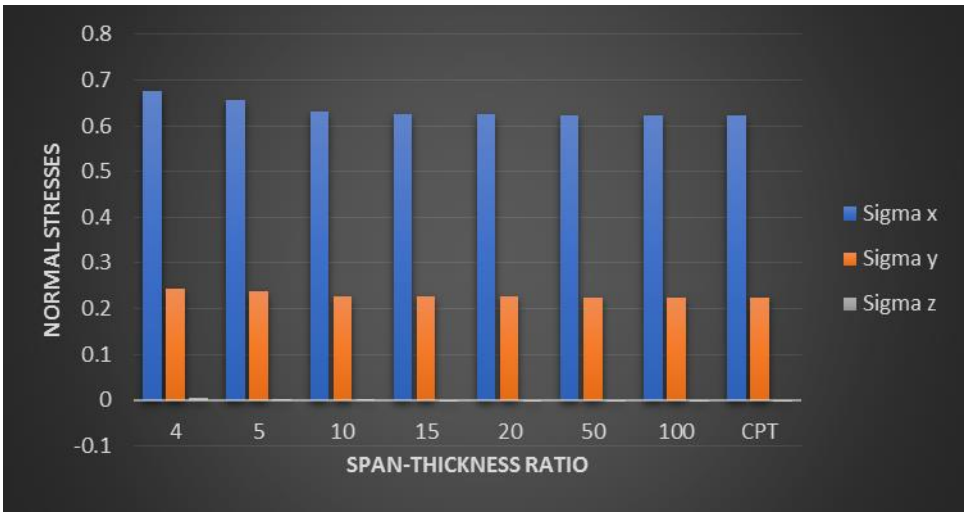

Fig. 7: Normal stresses and span-thickness ratio variation for SSFS plate with aspect ratio of 2.0

In Tables 1 and 2, Figure 8, the value of the shear stresses in the x-y plane (τ_{xy}) increased negatively as the span-depth ratio rises. The shear stresses in the x-z plane (τ_{xz}) decreased positively span-depth ratio of 4 to 50 and increased negatively in span-depth ratio of 100 and CPT. The parameters of shear-stresses in the y-z plane (τ_{yz}) decreased in the positive co-ordinate at a span - depth ratio of 4 to 50 and maintained a constant negative value of 0.0001 at span-depth ratio of 100 and CPT. The non-dimensional values of the shear stresses in Figure 3 were obtained at a length-breadth aspect ratio of 1.0.

In Figures 9, the non-dimensional parameters of the shear stresses in the x-y plane (τ_{xy}) increased in the negative direction with a constant negative value of 0.0925 a span - depth ratio of 50, 100 and CPT. The shear stresses in the x-z plane (τ_{xz}) reduced positively a span - depth ratio of 4 to 50 and increased negatively in span-depth ratio of 100 and CPT. The shear stresses in the y-z plane (τ_{yz}) decreased positively span-depth ratio of 4 to 20 and increased negatively span-depth ratios of 50, 100 and CPT.

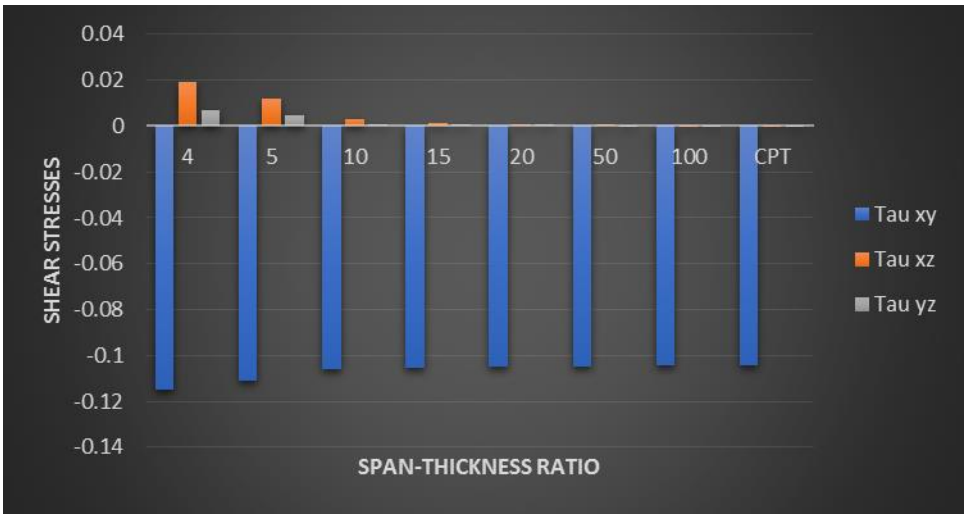

Fig. 8: Shear stresses and span-thickness ratio variation for SSFS plate with aspect ratio of 1.0

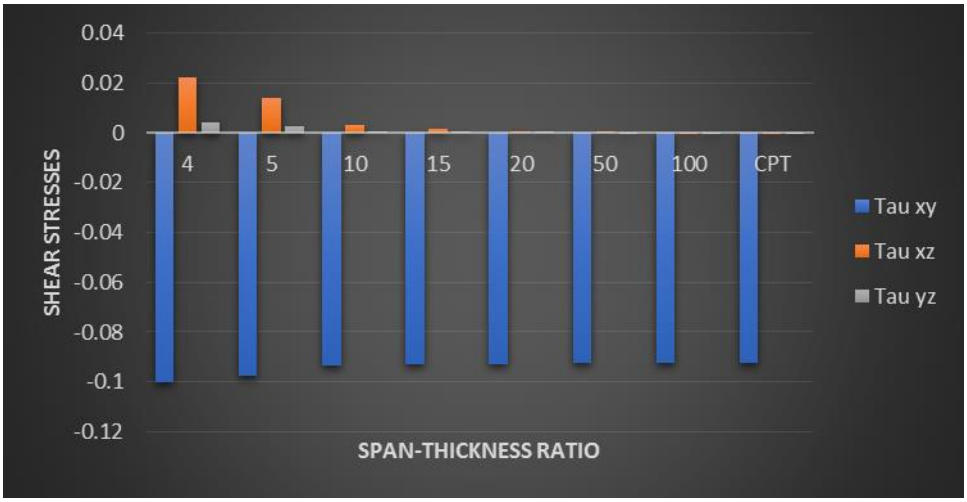

Fig. 9: Shear stresses and span-thickness ratio variation for SSFS plate with aspect ratio of 2.0

Succinctly, there exist categorically three rectangular plates. Thin plates can be considered as plates whose vertical shear stress and deflection do not vary largely from zero; their values being almost equivalent to CPT values. Thicker plates are classified as plates whose deflection and transverse shear stress differs greatly from zero. Moderately thick plates are plates that lie in between the thick and thin plates. Where a/t is the span-depth ratio for these categories of plate; $a/t \leq 10$ are thick plates, $15 \leq a/t \leq 50$ are moderately thick plate, while $a/t \geq 100$ are thin plates. This proof can be applied to depict the boundary between thin and thick plate. Therefore, it can be deduced from this study that thick plate is one whose span-depth ratio value is 4 up to 10.

Table 3 and Figure 10 represent the comparative values of deflection for previous works and the present work. It is observed that the present study which applied exact polynomial function with 3-D plate theory, provided accurately the deflection of the plate while previous studies which employed 2-D RPTs, underestimates and overestimates the out-of-plane displacement. The results obtained by Gwarah [49] differed more from the present study due to the use of the assumed displacement function. Although both Gwarah [49], Onyeka and Okeke [36] employed RPT, the solutions obtained by the later differed slightly from this study because the authors applied derived shape function. The non-dimensional deflection values of these studies decreased as the span-thickness ratio increased.

The divergence of the previous scholars with the present clearly shows that the 3-D model is exact and reliable, hence it should be espoused for accurate analysis of thick plates. The average percentage difference obtained between the present study and Gwarah [49] & Onyeka and Okeke [36] is 5.06% and 1.50% respectively, with an overall percentage variation of 3.28%. This means that at 95% and 98.5% confidence level, the values from the present study are equivalent to those of Gwarah [49] & Onyeka and Okeke [36] respectively. Statistically, this shows that the present approach can be embraced with confidence for an adequate analysis of rectangular SSFS

thick plate.

Table 3: Comparison of Non-dimensional deflection parameters of previous studies with present study results for SSFS square plate

$\alpha = \frac{a}{t}$	Gwarah [49]	Onyeka&Okeke [36]	Present Study [P.S]	Percentage difference (%) [P.S] and [49]	Percentage difference (%) [P.S] and [36]
4	0.00937	0.01004	0.00992	5.54435	1.20968
5	0.00877	0.00937	0.00925	5.18919	1.29730
10	0.00796	0.00856	0.00838	5.01193	2.14797
15	0.00781	0.00834	0.00822	4.98783	1.45985
20	0.00776	0.00828	0.00816	4.90196	1.47059
50	0.00770	0.00822	0.00810	4.93827	1.48148
100	0.00769	0.00821	0.00809	4.94437	1.48331
CPT	0.00769	0.00821	0.00809	4.94438	1.48331
Average percentage difference (%)				5.06	1.50
Overall percentage difference (%)				3.28	

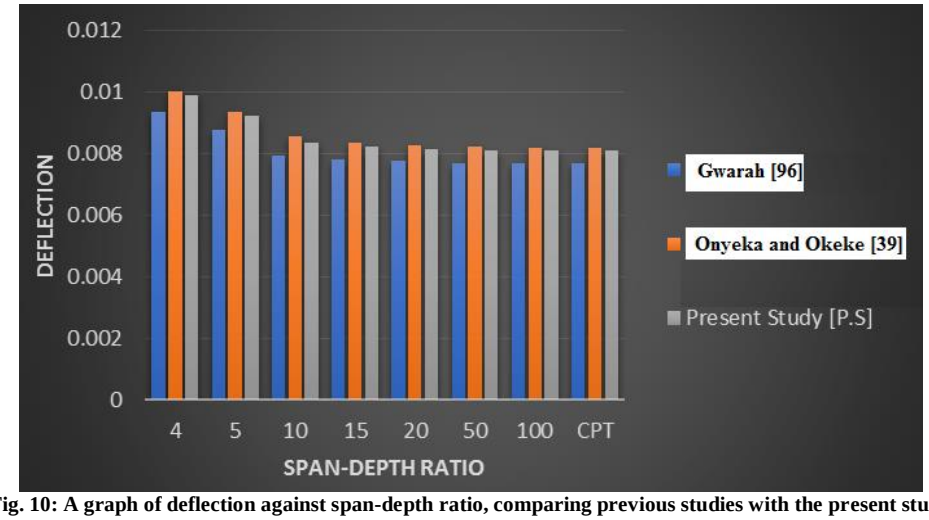

Fig. 10: A graph of deflection against span-depth ratio, comparing previous studies with the present study

5. Conclusion

The 3-D elasticity theory has been used to investigate the moments, displacements and stresses of thick rectangular plates with the following conclusions drawn from it:

a. The result obtained in this work which are compared with those of previous works revealed that 2-D refined plate theories are quite coarse for thick plate analysis. RPTs under-estimates and over predicts stresses, displacements and bending loads within the engineering allowable error of 3.28% for thick plate analysis.
b. The exact polynomial displacement functions offered closed-form solution for thick plate analysis.
c. The 3-D elasticity solution gave a more accurate and reliable solution compared refined plate theories and are recommended for the analysis of thick plate under the initial condition.
d. The model produced in this study can be employed to analyze plates at varying thicknesses and aspect ratio. Thus, the model produced in this study can be employed to analyze various categories of the plate.

Acknowledgements

We would like to acknowledge Ibearugbulem, Owus Mathias of Federal University of Technology, Owerri, Nigeria for providing the technical assistance during this research work.

References

[1] F. Onyeka, C. Nwa-David, E. Arinze, Structural imposed load analysis of isotropic rectangular plate carrying a uniformly distributed load using refined shear plate theory, *FUOYE Journal of Engineering and Technology*, Vol. 6, No. 4, pp. 414-419, 2021.

[2] F. Onyeka, B. O. Mama, C. Nwa-David, Application of variation method in three dimensional stability analysis of rectangular plate using various exact shape functions, *Nigerian Journal of Technology*, Vol. 41, No. 1, pp. 8–20-8–20, 2022.

[3] F. Onyeka, Direct analysis of critical lateral load in a thick rectangular plate using refined plate theory, *International Journal of Civil Engineering and Technology*, Vol. 10, No. 5, pp. 492-505, 2019.

[4] F. Onyeka, F. Okafor, H. Onah, Application of a new trigonometric theory in the buckling analysis of three-dimensional thick plate, *International Journal of Emerging Technologies*, Vol. 12, No. 1, pp. 228-240, 2021.

[5] E. S. Ventsel, T. Krauthammer, 2001, *Thin plates and shells: theory, analysis, and applications*, Marcel Dekker,

[6] K. Chandrashekhara, 2001, *Theory of plates*, Universities press,

[7] F. Onyeka, Effect of stress and load distribution analysis on an isotropic rectangular plate, *Arid Zone Journal of Engineering, Technology and Environment*, Vol. 17, No. 1, pp. 9-26, 2021.

[8] F. Onyeka, T. Okeke, C. Nwa-David, Static and buckling analysis of a three-dimensional (3-D) rectangular thick plates using exact polynomial displacement function, *European Journal of Engineering and Technology Research*, Vol. 7, No. 2, pp. 29-35, 2022.

[9] F. C. Onyeka, Stability analysis of three-dimensional thick rectangular plate using direct variational energy method, *Journal of Advances in Science and Engineering*, Vol. 6, No. 2, pp. 1-78, 2022.

[10] J. Reddy, Theory and Analysis of Elastic Plates and Shells, in *Proceeding of*.

[11] O. Festus, E. T. Okeke, W. John, Strain–Displacement expressions and their effect on the deflection and strength of plate, *Advances in Science, Technology and Engineering Systems*, Vol. 5, No. 5, pp. 401-413, 2020.

[12] P. Gujar, K. Ladhane, Bending analysis of simply supported and clamped circular plate, *International Journal of Civil Engineering*, Vol. 2, No. 5, pp. 69-75, 2015.

[13] F. Onyeka, F. Okafor, Buckling solution of a three-dimensional clamped rectangular thick plate using direct variational method, *building structure*, Vol. 1, pp. 3, 2021.

[14] J. Mantari, A. Oktem, C. G. Soares, A new trigonometric shear deformation theory for isotropic, laminated composite and sandwich plates, *International Journal of Solids and Structures*, Vol. 49, No. 1, pp. 43-53, 2012.

[15] F. Onyeka, D. Osegbowa, Stress analysis of thick rectangular plate using higher order polynomial shear deformation theory, *FUTO Journal Series–FUTOJNLS*, Vol. 6, No. 2, pp. 142-161, 2020.

[16] O. Ibearugbulem, F. C. Onyeka, Moment and stress analysis solutions of clamped rectangular thick plate, *European Journal of Engineering and Technology Research*, Vol. 5, No. 4, pp. 531-534, 2020.

[17] F. Onyeka, D. Osegbowa, E. Arinze, Application of a new refined shear deformation theory for the analysis of thick rectangular plates, *Nigerian Research Journal of Engineering and Environmental Sciences*, Vol. 5, No. 2, pp. 901-917, 2020.

[18] R. Mindlin, Influence of rotatory inertia and shear on flexural motions of isotropic, elastic plates, 1951.

[19] E. Reissner, The effect of transverse shear deformation on the bending of elastic plates, 1945.

[20] I. Sayyad, S. Chikalthankar, V. Nandedkar, Bending and free vibration analysis of isotropic plate using refined plate theory, *Bonfring International Journal of Industrial Engineering and Management Science*, Vol. 3, No. 2, pp. 40-46, 2013.

[21] F. C. Onyeka, T. E. Okeke, Analysis of critical imposed load of plate using variational calculus, *Journal of Advances in Science and Engineering*, Vol. 4, No. 1, pp. 13-23, 2021.

[22] C. Nwoji, H. Onah, B. Mama, C. Ike, M. Abd El Hady, A. Youssef, A. Bayoumy, Y. Elhalwagy, X. Wang, G. Ren, Ritz variational method for bending of rectangular Kirchhoff plate under transverse hydrostatic load distribution, *Mathematical Modelling of Engineering Problems*, Vol. 5, No. 1, pp. 1-10, 2018.

[23] R. Szilard, Theories and applications of plate analysis: classical, numerical and engineering methods, *Appl. Mech. Rev.*, Vol. 57, No. 6, pp. B32-B33, 2004.
[24] S. Timoshenko, S. Woinowsky-Krieger, 1959, *Theory of plates and shells*, McGraw-hill New York,
[25] C. Nwoji, B. Mama, C. Ike, H. Onah, Galerkin-Vlasov method for the flexural analysis of rectangular Kirchhoff plates with clamped and simply supported edges, *IOSR Journal of Mechanical and Civil Engineering*, Vol. 14, No. 2, pp. 61-74, 2017.
[26] C. Ike, Equilibrium approach in the derivation of differential equations for homogeneous isotropic Mindlin plates, *Nigerian Journal of Technology*, Vol. 36, No. 2, pp. 346-350, 2017.
[27] F. Onyeka, B. Mama, T. Okeke, Exact three-dimensional stability analysis of plate using a direct variational energy method, *Civil Engineering Journal*, Vol. 8, No. 1, pp. 60-80, 2022.
[28] N. G. R. Iyengar, 1988, *Structural stability of columns and plates / N.G.R. Iyengar*, Ellis Horwood ; Halsted Press, Chichester [England] : New York
[29] J. Mantari, C. G. Soares, Bending analysis of thick exponentially graded plates using a new trigonometric higher order shear deformation theory, *Composite Structures*, Vol. 94, No. 6, pp. 1991-2000, 2012.
[30] D. BHASKAR, A. G. Thakur, I. I. Sayyad, S. V. Bhaskar, Numerical Analysis of Thick Isotropic and Transversely Isotropic Plates in Bending using FE Based New Inverse Shear Deformation Theory, *International Journal of Automotive and Mechanical Engineering*, Vol. 18, No. 3, pp. 8882-8894, 2021.
[31] F. Y. Tash, B. N. Neya, An analytical solution for bending of transversely isotropic thick rectangular plates with variable thickness, *Applied Mathematical Modelling*, Vol. 77, pp. 1582-1602, 2020.
[32] Y. M. Ghugal, P. D. Gajbhiye, Bending analysis of thick isotropic plates by using 5th order shear deformation theory, *Journal of Applied and Computational Mechanics*, Vol. 2, No. 2, pp. 80-95, 2016.
[33] F. Onyeka, Critical lateral load analysis of rectangular plate considering shear deformation effect, *Global Journal of Civil Engineering*, Vol. 1, pp. 16-27, 2020.
[34] F. Onyeka, B. Mama, C. Nwa-David, Analytical modelling of a three-dimensional (3D) rectangular plate using the exact solution approach, *IOSR Journal of Mechanical and Civil Engineering*, Vol. 11, No. 1, pp. 10-22, 2022.
[35] F. Onyeka, E. T. Okeke, Analytical solution of thick rectangular plate with clamped and free support boundary condition using polynomial shear deformation theory, *Advances in Science, Technology and Engineering Systems Journal*, Vol. 6, No. 1, pp. 1427-1439, 2021.
[36] F. Onyeka, T. Okeke, New refined shear deformation theory effect on non-linear analysis of a thick plate using energy method, *Arid Zone Journal of Engineering, Technology and Environment*, Vol. 17, No. 2, pp. 121-140, 2021.
[37] A. Y. Grigorenko, A. Bergulev, S. Yaremchenko, Numerical solution of bending problems for rectangular plates, *International Applied Mechanics*, Vol. 49, pp. 81-94, 2013.
[38] F. Onyeka, T. Okeke, Elastic bending analysis exact solution of plate using alternative i refined plate theory, *Nigerian Journal of Technology*, Vol. 40, No. 6, pp. 1018–1029-1018–1029, 2021.
[39] F. Onyeka, B. Mama, Analytical study of bending characteristics of an elastic rectangular plate using direct variational energy approach with trigonometric function, *Emerging Science Journal*, Vol. 5, No. 6, pp. 916-928, 2021.
[40] A. Hadi, A. Rastgoo, A. Daneshmehr, F. Ehsani, Stress and strain analysis of functionally graded rectangular plate with exponentially varying properties, *Indian Journal of Materials Science*, Vol. 2013, 2013.
[41] O. Rahmani, S. Norouzi, H. Golmohammadi, S. Hosseini, Dynamic response of a double, single-walled carbon nanotube under a moving nanoparticle based on modified nonlocal elasticity theory considering surface effects, *Mechanics of Advanced Materials and Structures*, Vol. 24, No. 15, pp. 1274-1291, 2017.
[42] F. Ebrahimi, P. Haghi, Elastic wave dispersion modelling within rotating functionally graded nanobeams in thermal environment, *Advances in nano research*, Vol. 6, No. 3, pp. 201, 2018.
[43] M. Z. Nejad, A. Hadi, A. Rastgoo, Buckling analysis of arbitrary two-directional functionally graded Euler–Bernoulli nano-beams based on nonlocal elasticity theory, *International Journal of Engineering Science*, Vol. 103, pp. 1-10, 2016/06/01/, 2016.
[44] Y. Z. YÜKSEL, Ş. D. AKBAŞ, Free vibration analysis of a cross-ply laminated plate in thermal environment, *International Journal of Engineering and Applied Sciences*, Vol. 10, No. 3, pp. 176-189, 2018.
[45] Y. Z. Yüksel, D. Akbaş, Hygrothermal stress analysis of laminated composite porous plates, *Structural Engineering and Mechanics*, Vol. 80, No. 1, pp. 1-13, 2021.
[46] Y. Z. Yüksel, Ş. D. Akbaş, Buckling analysis of a fiber reinforced laminated composite plate with porosity, *Journal of Computational Applied Mechanics*, Vol. 50, No. 2, pp. 375-380, 2019.

[47] Ş. D. AKBAŞ, Stability of a non-homogenous porous plate by using generalized differantial quadrature method, *International Journal of Engineering and Applied Sciences*, Vol. 9, No. 2, pp. 147-155, 2017.

[48] Ş. AKBAŞ, Static analysis of a nano plate by using generalized differential quadrature method, *International Journal of Engineering and Applied Sciences*, Vol. 8, No. 2, pp. 30-39, 2016.

[49] L. S. Gwarah, Application of shear deformation theory in the analysis of thick rectangular plates using polynomial displacement functions, *PhD Thesis Presented to the School of Civil Engineering, Federal University of Technology, Owerri, Nigeria*, 2019.